






Research Article

A Wideband Tightly Coupled Array for Omnidirectional Pattern Synthesis

Manuel Luciarini ¹, **Domenico Gaetano** ², **Christian Canestri** ², **Cosmo Mitrano** ²,
Walter Fuscaldo ³ and **Alessandro Galli** ¹

¹Department of Information Engineering Electronics and Telecommunications, Sapienza University, Rome, Italy

²Elatronica S.p.A, Via Tiburtina, Rome 13700, Italy

³Istituto per la Microelettronica e Microsistemi, Consiglio Nazionale delle Ricerche, Rome, Italy

Correspondence should be addressed to Manuel Luciarini; manuelluciarini@gmail.com

Received 23 December 2021; Revised 13 March 2022; Accepted 26 March 2022; Published 22 April 2022

Academic Editor: Stefano Selleri

Copyright © 2022 Manuel Luciarini et al. This is an open access article distributed under the Creative Commons Attribution License, which permits unrestricted use, distribution, and reproduction in any medium, provided the original work is properly cited.

This work presents the design of a wideband circular tightly coupled array for omnidirectional pattern generation. The proposed array works over an 8:1 bandwidth, providing very high performance in terms of active reflection coefficient, realized gain, and omnidirectional patterns with reduced ripples. The array is composed of 32 low-profile, self-complementary, bow-tie elements displaced around a metallic mast. The capacitive coupling between neighbouring elements and the implementation of a properly designed frequency selective surface allow for increasing the electrical length of each antenna while compensating for the inductive effect of the metallic mast, according to the tightly coupled and connected arrays theory. A cover layer is then inserted to improve the average gain on the azimuthal plane. Time-domain simulation results confirm the validity of the proposed approach and implementation.

1. Introduction

During the last years, tightly coupled arrays (TCAs) attracted a lot of interest owing to their advantages, such as wide bandwidth and good radiative performance [1, 2]. Devices based on TCAs are expected to find applications in various contexts such as radar systems, 5G mobile communications, and the Internet of Things (IoT) [3]. The concept of TCAs was originated from Wheeler's (and then Munk's) idea of the current sheet [3], which consists in placing the adjacent radiating elements close enough to deliberately generate a strong capacitive coupling. The latter effect is able to counteract the inductive effect of the ground plane (which is supposed to be close to the radiating elements) and increase their electrical length, resulting in a higher radiation resistance at low frequencies. Munk's array achieved 9:1 bandwidth and has been regarded as a benchmark since 2009. Since that time, TCAs have been used in numerous applications in UHF and SHF bands with

additional elements (substrates, superstrates, and coupling structures) to improve TCAs in terms of scan performance, costs, low cross-polarization, and easiness of fabrication.

Numerous designs [3–5] have proven successful in providing all the above-mentioned features whilst ensuring proper matching (VSWR less than 2–3.5) in a rather wide bandwidth (from 1.6:1 to 21:1). In this regard, Table 1 shows a summary of the state of the art of TCAs (2018) in terms of achieved bandwidth (BW), voltage standing-wave ratio (VSWR), radiation efficiency (η_{rad}), and specific features. They have been sorted in ascending order by their bandwidth. Further details about the referred designs can be found in [6–20]. All of them incorporate specific structures to enhance the array bandwidth. The recently published papers [12, 15, 20] are an interesting reference for the work proposed in this manuscript, as they proposed similar bandwidths (from 5:1 to 9:1) achieved with similar coupling techniques. But, on the whole, [18] has been the most important reference because its extremely promising results

TABLE 1: State of the art of TCAs.

| BW | VSWR | η_{rad} | Features | Ref |
|--------|-------------|---------------------|-------------------------------------|------|
| 1.6:1 | <2 | 93% (B.S.) | Shorted edge terminations | [6] |
| 2.5:1 | <2 | N.M. | Parasitic ring loading | [7] |
| 3:1 | <2.1 (B.S.) | N.M. | PUMA | [8] |
| 3.3:1 | <3 | N.M. | Octagonal ring element | [9] |
| 5:1 | <2.1 (B.S.) | N.M. | PUMA | [10] |
| 5:1 | <2 (B.S.) | N.M. | | [11] |
| 5:1 | | >60% | Metasurface | |
| 6:1 | <3 | 85% | Capacitive overlaps | [12] |
| 6.1:1 | <3.2 | 65%–80% | Maximum scan angle; FSS superstrate | [13] |
| 7.35:1 | <2.65 | N.M. | | [14] |
| 9:1 | <3.4 | N.M. | Resistive FSS | [15] |
| 10:1 | <2 (B.S.) | N.M. | Spiral element | [16] |
| 13.5:1 | <2.5 (B.S.) | 60%–70% | Substrate loading | [17] |
| 21:1 | <3 (B.S.) | 73% | Resistive FSS substrate | [18] |

*B.S.: broadside scan. **N.M.: not mentioned. ***PUMA: planar ultrawideband modular antenna.

showed a very large bandwidth achieved through an array of bow-tie elements located between an FSS (frequency selective surface) and a superstrate. The same techniques have been applied to this work too.

All the above-mentioned works describe the design of planar arrays with a ground plane, and their results have not been extended to more specific structures such as circular TCAs around a metallic mast. Here, the aim is to obtain similar results with these kinds of structures while satisfying further requirements, such as omnidirectional patterns with controlled gain ripples on the elevation plane over the operating bandwidth.

The proposed work presents the design of an original architecture consisting of a circular tightly coupled array that works over an 8:1 bandwidth (from $1.1f_0$ to $9f_0$), defined as the frequency range where the average realized gain is greater than -5 dBi. This definition has been chosen because the realized gain (which includes the loss due to the impedance matching) was the relevant figure of merit for such an antenna. According to this definition, the actual bandwidth is presumably wider, as the average realized gain is still higher than 4 dBi at the upper edge frequency $9f_0$. However, the array performance for frequencies higher than $9f_0$ is beyond the scope of this work and thus has not been analyzed. It is worth stressing here that f_0 can be any frequency in the microwave range subject to the availability of the thicknesses of the commercial laminates used in the antenna design. The dimensions of the array design are thus reported in terms of the operating wavelength and will scale accordingly. Still, the presented results have been obtained by choosing f_0 in the licensed NATO E-Band, that is, within the 2–3 GHz frequency range.

The device is expected to be mounted around a metallic mast, providing a modular solution that can be implemented on several platforms (naval or terrestrial). Omnidirectional patterns with controlled ripples are required to provide a 360° analysis of all incident signals in the azimuthal plane with half-power beamwidth (HPBW) higher than 20° on the elevation plane. A circular array consisting of 32 wideband horizontally

polarized bow-tie antennas has been chosen to comply with the above-mentioned requirements.

The paper is organized as follows. Section 2 describes the circular array design. Section 3 illustrates the design of a proper frequency selective surface (FSS) to compensate for most inductive effects and a superstrate to improve the average realized gain in the azimuthal plane. Section 4 shows the most relevant full-wave results. Concluding remarks are finally drawn in Section 5.

2. Array Design

The proposed array is composed of 32 self-complementary horizontally polarized bow-tie antennas placed on a TG24/2000 Trelleborg Eccofloat [21] ($\epsilon_r = 1.45$ and $\tan \delta = 0.002$) circular substrate around a metal mast. The array is expected to be used at frequencies lower than $9f_0$ and has a bandwidth (average realized gain greater than -5 dBi on the azimuthal plane) ranging from $1.1f_0$ to $9f_0$ (8:1). Figure 1 shows the array structure with the relevant reference system.

The mast has a radius $R_M = 0.58\lambda_{\text{max}}$ (where $\lambda_{\text{max}} = c/f_0$, with c speed of light in vacuum) and a length of $4\lambda_{\text{max}}$ (these are typical values for masts used in, e.g., naval platforms). The device can be adapted to masts with different radii by varying the number of elements in order to guarantee an omnidirectional pattern (low realized gain ripple in the elevation plane).

Figure 2 shows the realized gain ripple on the azimuthal plane for 16 and 32 elements of the array. The ripple is evaluated as the difference between the maximum and the minimum realized gain for each fixed frequency and elevation plane. Considering 32 radiating elements of length $0.112\lambda_{\text{max}}$, a realized gain ripple lower than 8 dB for elevation 0° plane is obtained. It is seen that if, with the same mast radius, 16 bow-tie elements of double-length ($0.224\lambda_{\text{max}}$) are used, the realized gain ripple in the azimuthal plane turns unacceptable for $f > 3.5f_0$.

A self-complementary bow-tie antenna has been chosen as the radiating element. It consists of a pair of metal triangles printed on a dielectric substrate and achieves a good wideband performance while exhibiting lightweight and a simple planar

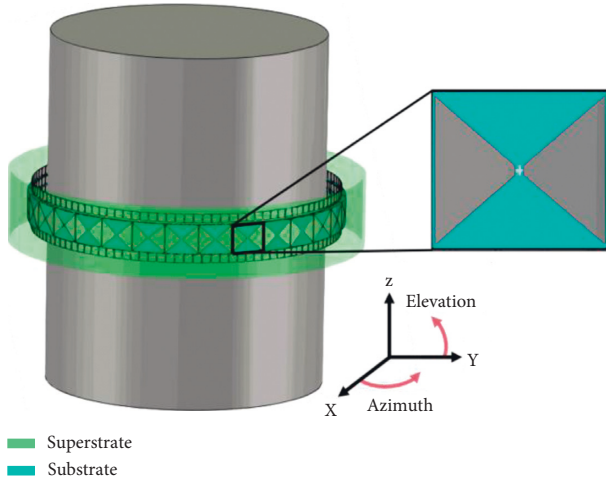


FIGURE 1: Tightly coupled array under analysis: 3-D model.

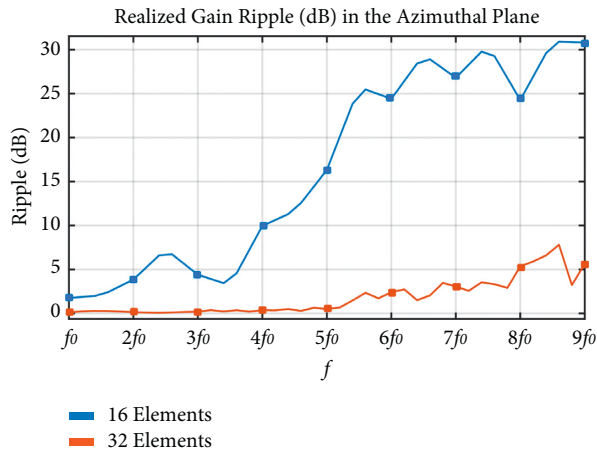


FIGURE 2: Realized gain ripple in the azimuthal plane at different frequencies for 16 and 32 elements arrays. The array radius has been kept fixed to $0.58\lambda_{\max}$.

conformable structure [22]. Each bow-tie antenna is $\lambda_{\max}/9$ long in order not to increase the realized gain ripple at high frequencies. A bow-tie flare angle equal to 77.3° has been chosen to guarantee, together with a low-permittivity substrate, a $200\ \Omega$ input impedance [23]. The distance between each bow-tie antenna and the mast has been optimized through various accurate simulations (time-domain simulation throughout the whole bandwidth f_0-9f_0 to analyze the behaviour of the overall structure and frequency-domain simulation at $3.215f_0$ to analyze the parallel LC resonance between the metal mast and the designed FSS) in order to provide a reduced inductive loading effect on each radiating element, which limits the bandwidth by lowering the radiation resistance, particularly in the low-frequency band (approximately from $1.1f_0$ to $3.5f_0$).

Unfortunately, whilst long bow-tie antennas show wideband performance, the same does not occur if the antenna length is not much greater than the operating wavelength. Hence, in the case of our interest, only in the higher frequency band ($3f_0-9f_0$), good matching is achieved.

Figure 3 shows how the input reflection coefficient magnitude of a single bow-tie antenna gradually increases as its length L is reduced. If a bow-tie antenna with $L=0.56\lambda_{\max}$ ensures $|S_{11}|<-10\text{ dB}$ throughout the bandwidth, the same does not apply for the case with $L=0.11\lambda_{\max}$, where $|S_{11}|<-5\text{ dB}$ occurs from $3f_0$ (and from $4f_0$ if a metallic mast close to the antenna is placed). This problem has been solved thanks to capacitive coupling between adjacent antennas aimed at increasing the single antenna electrical length and compensating for the mast loading effect. Each antenna has been supplied by a discrete port of $200\ \Omega$ that is equal to the average radiation resistance of a bow-tie antenna in free-space with a 77.3° flare angle. A $0.0136\lambda_{\max}$ thickness TG24/2000 substrate has been chosen to achieve an average input impedance of $200\ \Omega$ for each bow-tie element.

An approximate transmission line model has been used to design an FSS able to compensate for the mast inductance. Assuming the metal mast to be in the antenna far-field region in the receiving mode (which is verified until $4.25f_0$) and focusing only on the wave propagation along the normal direction to each bow-tie antenna, the equivalent circuit shown in Figure 4 has been considered.

In this approximate model, each antenna sees an equivalent load equal to the parallel connection between the free-space impedance representing the upper space and the input impedance of the lower space transmission line loaded on the mast. In the considered device, through the previous transmission-line model, the mast can be shown to be an equivalent inductor of 13.6 nH . Its effect is to “short” the antenna output port in $1.1f_0-3.5f_0$ approximately, causing an abrupt drop in radiation resistance at the antenna input port.

In order to obtain a controlled omnidirectional pattern exploiting the TCA theory, the distance between the phase centres of the chosen bow-tie antennas should be less than $0.11\lambda_{\max}$, according to circular array theory [24]. Therefore, the radiation resistance of the single bow-tie element is further reduced.

Tight coupling is provided between adjacent elements in order to compensate for the mast inductive effect and increase the radiation resistance, according to Munk’s and Wheeler’s current sheet concept [25].

In Section 4, it is described how the low-frequency behaviour of the input active reflection coefficient can indeed be strongly improved through this technique [26]. The array is able to take advantage of the extra inductance from the metal mast to resonate with the capacitive impedance of the coupled radiating elements, resulting in a wider bandwidth.

3. FSS and Superstrate Design

A capacitive FSS [27] can be introduced to further compensate for the mast inductive effect in the low-frequency band. The FSS has been realized with properly displaced capacitive metal squares providing a good matching compensation in $1.1f_0-3f_0$ at the expense of mitigating the higher frequency performances. An active VSWR <3.57 is achieved in $1.6f_0-9f_0$ owing to TCA and

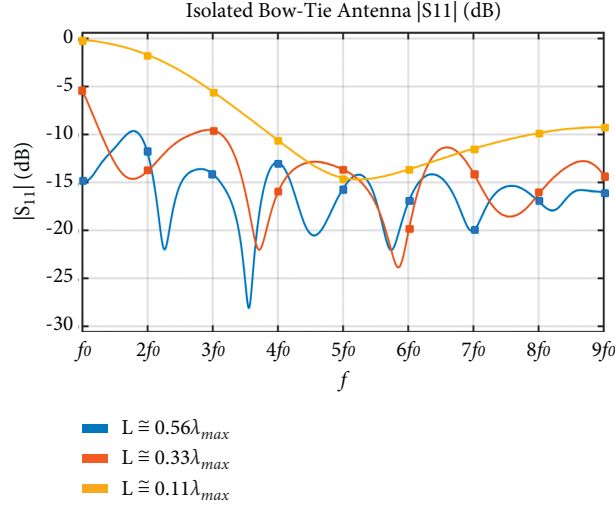


FIGURE 3: Input reflection coefficient magnitude $|S_{11}|$ (dB) for an isolated bow-tie antenna with 77.3° flare angle supplied with a 200 discrete source. Three different antenna lengths have been considered.

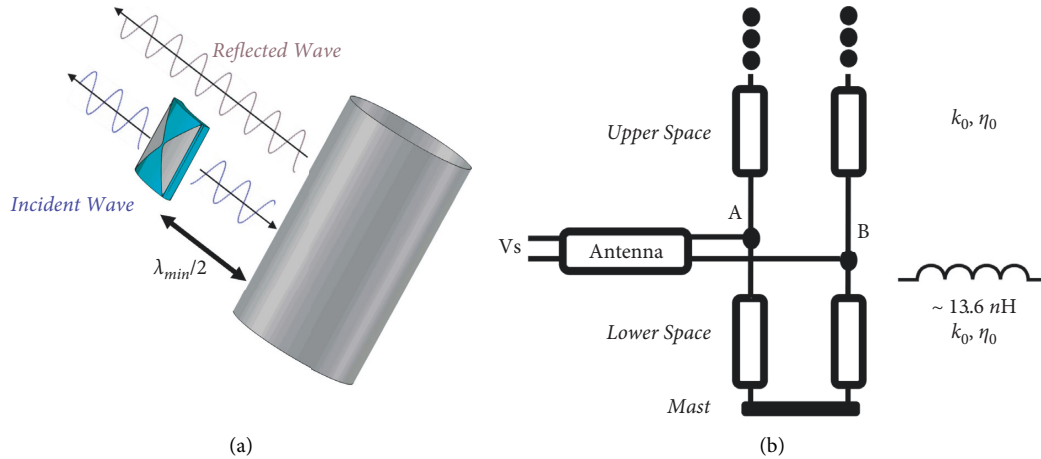


FIGURE 4: (a) CAD model of a single bow-tie antenna with metal mast and (b) transmission-line equivalent model.

FSS (see Section 4). Such a result has been obtained through time-domain simulation (from f_0 to $9f_0$) of the entire structure. Moreover, the FSS allows us to control the destructive interference between the radiated waves and the reflected waves from the metal mast, especially around its central frequency.

An FSS made of an array of square patches has been chosen (see Figure 5). They have been designed with unit cell subwavelength period $D = 0.03\lambda_{\max}$ and spacing $w = 0.0033\lambda_{\max}$ to achieve an equivalent input capacitance of 0.045 pF for TEM incidence according to the following equations [28]:

$$Z_s^{\text{TEM}} = -j \frac{\eta_0}{2\alpha\sqrt{\epsilon_{\text{eff}}}} \quad (1)$$

where ϵ_{eff} is the relative effective permittivity of the uniform host medium and α is the grid parameter and can be expressed as follows:

$$\alpha = \frac{k_0\sqrt{\epsilon_{\text{eff}}}}{\pi} D \cdot \ln \left[\frac{1}{\sin(\pi w/2 D)} \right]. \quad (2)$$

Such a capacitance has been designed to compensate for the inductive behaviour of the metal mast until $4f_0$. Parallel LC resonance occurs at about $3.215f_0$.

In order to increase the array average realized gain on the azimuthal plane, a superstrate has been inserted in front of the radiating elements at a distance of $0.059\lambda_{\max}$. This well-known issue has been investigated in [29, 30] and shows how a properly designed high-permittivity superstrate can increase the antenna directivity at the expense of a reduction in bandwidth. More recently, the same phenomena have been analyzed for wideband applications [5, 18, 31, 32]. Therefore, the antenna directivity can be approximated as a function of the ratio between the dielectric permittivity of the superstrate and that of the substrate (see, e.g., [24]). Moreover, it has recently been shown [33, 34] that when the FSS is lossy, the

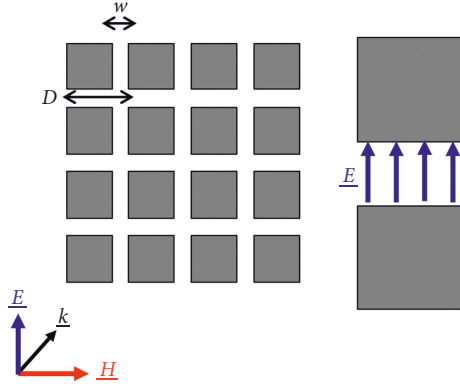


FIGURE 5: A capacitive FSS made with square metal patches.

position that maximizes the gain at the broadside is no longer the substrate-superstrate interface but shifts towards the middle plane of the substrate. A higher permittivity superstrate (ROGERS TC350; $\epsilon_r = 3.5$ and $\tan \delta = 0.002$ [35]) has been chosen, and by means of parametric time-domain simulations on CST MWS, it has been shown able to guarantee an improvement of 2 dBi of the average realized gain over the azimuthal plane.

4. Array Performance

The single element structure with the FSS designed in Section 3 is depicted in Figure 6 in an array configuration. As described, each bow-tie antenna has been designed with a 77.3° flare angle to show an average input radiation resistance of 200Ω throughout the bandwidth [23]. The bow-tie antenna length L has been fixed to $0.11\lambda_{\max}$ to guarantee a circular spacing between adjacent radiating elements small enough to keep the realized gain ripple below 8 dB (the overall spacing between array elements is d). A coupling distance $G = 0.0027\lambda_{\max}$ has been shown to be the optimal trade-off for such a device between the increase of the electrical length and the increase of the transmission coefficients S_{ij} , $i \neq j$.

As shown in Figure 7, the low-density synthetic foam TG24/2000 has been chosen as a substrate to provide a low effective permittivity and minimize unwanted coupling whilst guaranteeing the desired radiation resistance with the bow-tie dimensions previously chosen. The array main dimensions are indicated in Table 2. The distance $u = 0.053\lambda_{\max} = 0.48\lambda_{\min}$ between each bow-tie antenna and the metal mast is slightly less than $\lambda_{\min}/2$ to avoid destructive interference at $9f_0$ whilst minimizing the inductive effect of the metal mast by keeping it far enough. Finally, the higher permittivity superstrate ROGERS TC3502 has been inserted to increase the antenna realized gain in addition to the array factor enhancement. Simulations have shown that a 2 dBi average increase of the realized gain in the azimuthal plane may be reached without compromising the bandwidth. This result is achieved through the reduction of the elevation beamwidth due to the added superstrate.

Figure 8 depicts the three main array configurations that have been considered in the simulations. The initial model consists of a simple TCA without additional

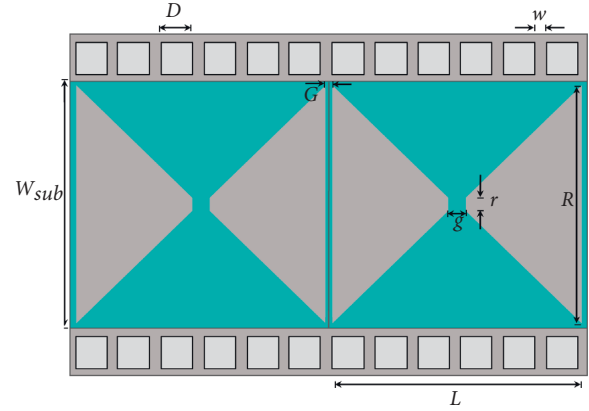


FIGURE 6: Array front view with single bow-tie elements, FSS, and mast. The array's main dimensions are shown.

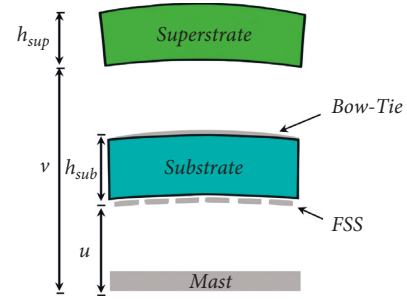


FIGURE 7: Array view with single bow-tie element, substrate, superstrate, FSS, and mast. The array's main dimensions are shown.

TABLE 2: Array parameters.

| Size (fraction of λ_{\max}) | Description |
|--------------------------------------|---------------------------|
| $d = 0.1150$ | Bow-tie centres spacing |
| $g = 0.0017$ | Feed gap |
| $L = 0.1120$ | Bow-tie length |
| $R = 0.090$ | Bow-tie width |
| $G = 0.0027$ | Bow-tie edges spacing |
| $D = 0.03$ | FSS side |
| $w = 0.0033$ | FSS spacing |
| $h_{\text{sup}} = 0.0133$ | Superstrate thickness |
| $h_{\text{sub}} = 0.0136$ | Substrate thickness |
| $RM = 0.5801$ | Mast radius |
| $W_{\text{sub}} = 0.1067$ | Substrate width |
| $v = 0.1063$ | Superstrate-mast distance |
| $u = 0.0053$ | FSS-Mast distance |

elements. Then an FSS has been added, and the final structure with both FSS and superstrate has been considered. All the following simulation performances refer to those three configurations.

The final array design achieves an active input reflection coefficient of $|\Gamma_{\text{in}}| < -5$ dB (i.e., active VSWR < 3.57) from $1.55f_0$ to $9f_0$, as illustrated in Figure 9 (see the yellow curve). The frequency response of the input reflection coefficient of a single bow-tie antenna close to the metallic mast (see the blue curve) presents a considerable mismatch around $1.1f_0$ – $3f_0$. Placing such an antenna in a TCA configuration increases its electrical length providing a good matching

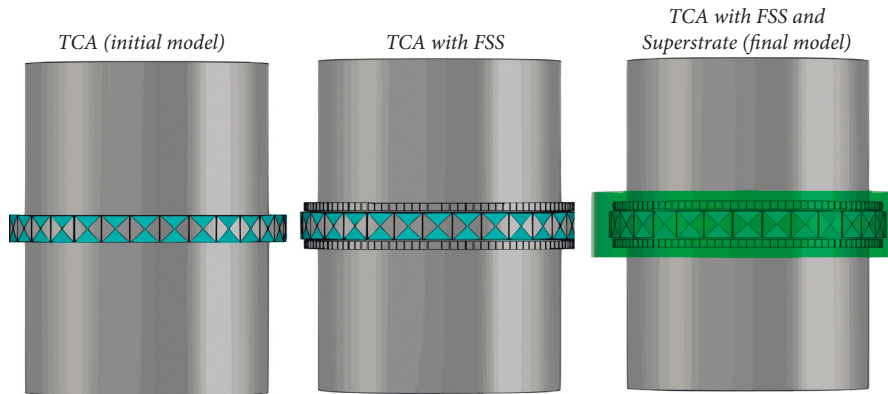


FIGURE 8: Main array configurations compared in terms of simulated performances.

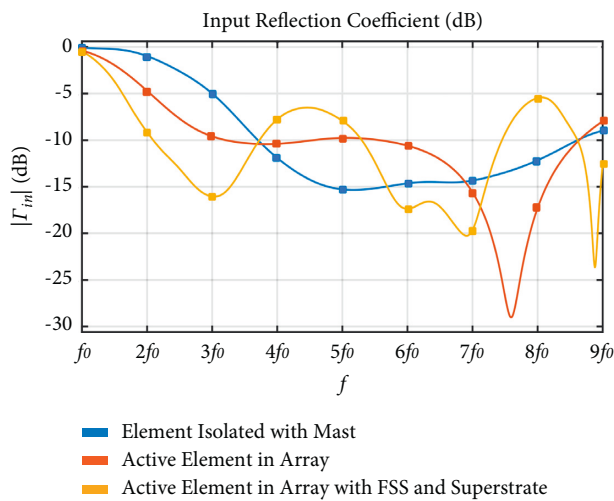


FIGURE 9: Frequency responses of the absolute value of the input reflection coefficient (dB).

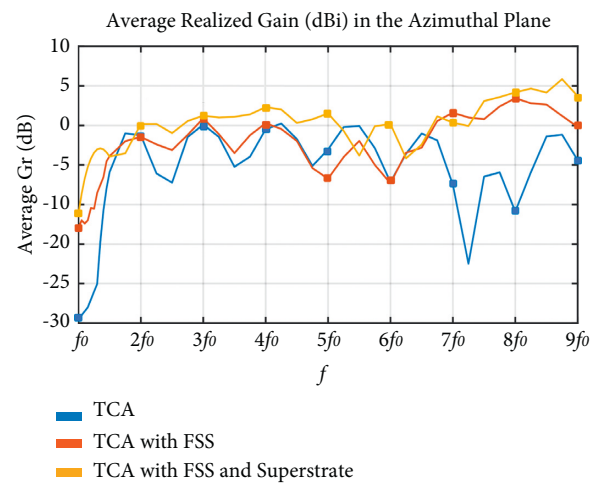


FIGURE 10: Frequency response of the average realized gain (in dBi) in the azimuthal plane for different TCA solutions. Only the horizontal (azimuth) polarization has been considered.

from $2.4f_0$ (see the red curve). The low-frequency performance is further improved by inserting the designed FSS for a greater compensation of the parasitic inductance of the metal mast (see the yellow curve).

Figure 10 illustrates the frequency response of the average realized gain over the azimuthal plane for the horizontal polarization (HP). The realized gain over the azimuthal plane $G_r(Az, El=0^\circ)$ is defined as the realized gain pattern (function of the azimuth and elevation angles) evaluated at 0° elevation (azimuthal plane). Such a function of the azimuth angle is of great interest as our purpose was to design an omnidirectional antenna in the azimuthal plane ($G_r(Az, El=0^\circ) = \text{constant}$). Its average value, analyzed for each frequency of interest, is a good figure of merit for the design of such an antenna. The blue curve shows the performances achieved by the TCA made of 32 bow-tie elements. If a proper FSS is added, a significant increase in the mean realized gain is observed in $6.5f_0-9f_0$ (see the orange curve). It is possible to explain this phenomenon from a theoretical viewpoint. The partial shielding of the wave reflected from the mast is a possible cause of this behaviour. In particular, in the upper-

frequency band, it would destructively interfere with the wave radiated by each antenna as the distance from the mast approaches $\lambda/2$. In brief, the FSS suppresses the $\lambda/2$ resonance induced by the metal mast. Finally, the insertion of the aforementioned superstrate allows for increasing the mean realized gain up to 2 dBi (see the yellow curve). The resulting device provides an average realized gain in the azimuth plane between -4.1 dBi and $+5.8$ dBi over the whole band $1.2f_0-9f_0$.

The frequency behaviour of the realized gain ripple in the azimuthal plane is shown in Figure 11. The realized gain ripple in the azimuthal plane is defined as the deviation in dB between the maximum and minimum value of the realized gain in the azimuthal plane $G_r(Az, El=0^\circ)$. The initial model of the TCA has a ripple peak higher than that of the final versions with the same $(0.115\lambda_{\max})$ circular spacing between adjacent bow-tie antennas. Those peaks are significantly lowered by the insertion of the FSS (red curve), which reduces the destructive interference, thus mitigating the minimum points in the radiation pattern. A small increase of the ripple (less than 3 dB) is observed for $4f_0 < f < 6f_0$ and $f > 8f_0$ when the superstrate is added. Nevertheless, the final

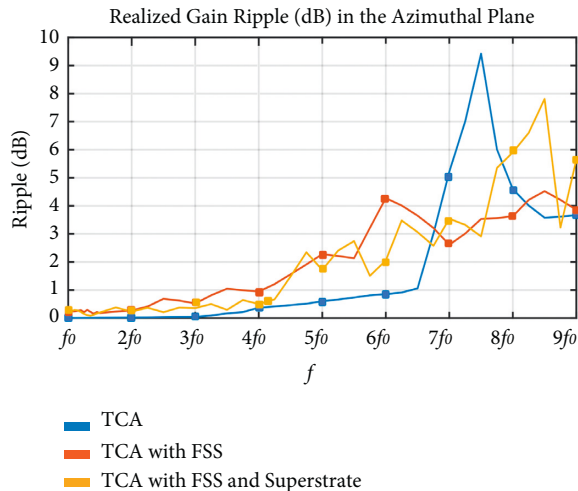


FIGURE 11: Frequency response of the realized gain ripple in the Azimuth plane.

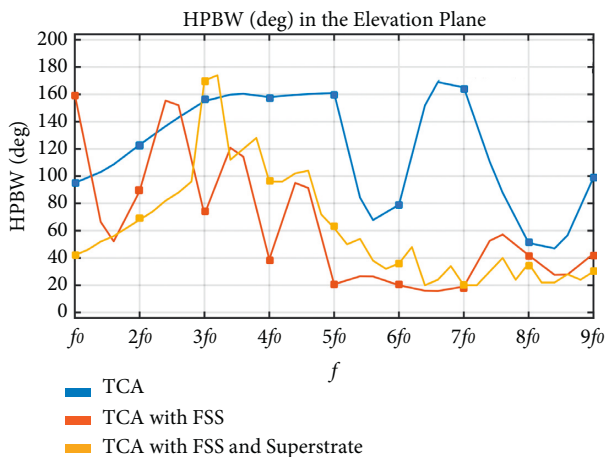


FIGURE 12: Frequency response of the HPBW in the elevation plane.

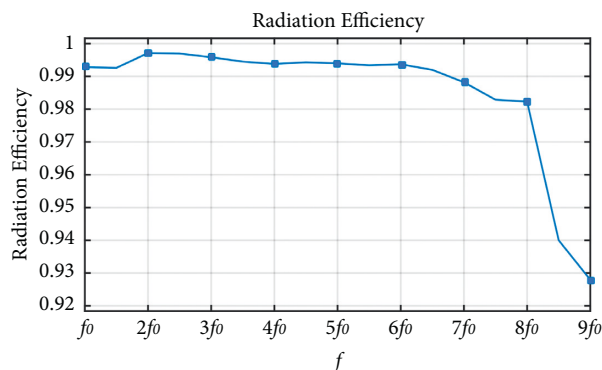


FIGURE 13: Frequency response of the radiation efficiency of the proposed array.

device presents a realized gain ripple lower than 8 dB over the entire frequency band.

The frequency response of the half-power beamwidth (HPBW) in the elevation plane for the horizontal

polarization is shown in Figure 12. The proposed final array achieves HPBW $>20^\circ$ over the desired bandwidth.

All previous results have been obtained by choosing an 18 μm -thick copper layer as the metal conductor for each bow-tie antenna, the metal mast, and the FSS. These results perfectly overlap with those obtained with PEC materials. The insertion of low-loss materials to counteract parasitic effects results in a very high radiation efficiency compared to that achieved in several designs shown in Table 1 including RFSS (resistive FSS) [3]. Figure 13 shows the frequency response of the radiation efficiency for the proposed array. It is higher than 93% throughout the entire bandwidth.

5. Conclusion

In this paper, an original architecture consisting of 32 bow-tie elements arranged in a circular array configuration surrounding a metallic mast has been proposed, providing a modular solution that can be implemented on several platforms (naval or terrestrial). We exploited the concepts of tightly coupled antenna theory to achieve satisfactory performance in terms of realized gain ripple and radiation efficiency over an 8:1 bandwidth. The novelty of this work consists in the application of the current sheet concept originated from Munk's and Wheeler's works to a circular array used for the synthesis of an omnidirectional radiation pattern around a metallic mast.

The insertion of an FSS and a proper dielectric superstrate, together with an optimal degree of capacitive coupling, resulted in a good performance in the whole bandwidth of interest. Nonresistive compensations have been used to counteract the mast parasitic inductance and increase the radiation resistance, resulting in a very high radiation resistance throughout the bandwidth. The final antenna has provided an average realized gain in the azimuth plane between -5 dBi and $+5.8\text{ dBi}$, with ripple lower than 8 dB, an HPBW $>20^\circ$, and a radiation efficiency higher than 93% over the whole band $1.1f_0-9f_0$, with f_0 in E-Band. Future works include the design of a tapered wide-band microstrip BALUN with the purpose of matching the 200 Ω bow-tie input impedance to a 50 Ω microstrip line. In the final structure, 32 BALUNs, passing through 32 pre-drilled holes inside the mast, would supply the single elements of the array. Such a feed network would be contained almost entirely inside the metal mast already taken into account in the array design, hence with minimal effect on the overall radiation pattern and array performances.

Data Availability

All data used to support the findings of this study are available from the corresponding author upon request.

Conflicts of Interest

The authors declare that they have no conflicts of interest.

References

- [1] Y. Sui, Y. Li, and L. Zhao, "A 7:1 bandwidth tightly coupled antenna array with large angle scanning," in *Proceedings of the 2018 International Symposium on Antennas and Propagation (ISAP)*, pp. 1-2, IEEE, Busan, Korea, October 2018.
- [2] C. Canestri, D. Gaetano, P. Bia, A. Manna, and C. Mitrano, "An innovative UWB connected array for multifunctional applications," in *Proceedings of the 2019 IEEE International Symposium on Antennas and Propagation and USNC-URSI Radio Science Meeting*, pp. 517-518, IEEE, Atlanta, GA, USA, July 2019.
- [3] Y. Zhou, F. Zhu, S. Gao et al., "Tightly coupled array antennas for ultra-wideband wireless systems," *IEEE Access*, vol. 6, pp. 61851-61866, 2018.
- [4] X. Liang, W. Yin, A. Chen et al., "Ultrawideband, wide scanning stripline-fed tightly coupled array antenna based on parallel-dipole elements," *Sensors*, vol. 20, no. 18, p. 5065, 2020.
- [5] I. Tzanidis, K. Sertel, and J. L. Volakis, "UWB low-profile tightly coupled dipole array with integrated balun and edge terminations," *IEEE Transactions on Antennas and Propagation*, vol. 61, no. 6, pp. 3017-3025, 2013.
- [6] J. A. Kasemodel, C.-C. Chen, and J. L. Volakis, "Wideband planar array with integrated feed and matching network for wide-angle scanning," *IEEE Transactions on Antennas and Propagation*, vol. 61, no. 9, pp. 4528-4537, 2013.
- [7] H. H. Vo, C.-C. Chen, P. Hagan, and Y. Bayram, "A very low-profile UWB phased array antenna design for supporting wide angle beam steering," in *Proceedings of the 2016 IEEE International Symposium on Phased Array Systems and Technology (PAST)*, pp. 1-8, IEEE, Waltham, MA, USA, October 2016.
- [8] S. S. Holland, D. H. Schaubert, and M. N. Vouvakis, "A 7-21 GHz dual-polarized planar Ultrawideband modular antenna (PUMA) array," *IEEE Transactions on Antennas and Propagation*, vol. 60, no. 10, pp. 4589-4600, 2012.
- [9] Y. Zhang and A. K. Brown, "Octagonal ring antenna for a compact dual-polarized aperture array," *IEEE Transactions on Antennas and Propagation*, vol. 59, no. 10, pp. 3927-3932, 2011.
- [10] S. S. Holland and M. N. Vouvakis, "The planar Ultrawideband modular antenna (PUMA) array," *IEEE Transactions on Antennas and Propagation*, vol. 60, no. 1, pp. 130-140, 2012.
- [11] H. Huang, K. Xiao, L. Ding, S. Wang, and S. Chai, "Ultrawideband tightly coupled array for multiband communications at S-X frequencies," in *Proceedings of the 2016 IEEE International Workshop on Electromagnetics: Applications and Student Innovation Competition (iWEM)*, pp. 1-3, IEEE, Nanjing, China, May 2016.
- [12] M. Carvalho and J. L. Volakis, "Deployable rigid-flexible tightly coupled dipole array (RF-TCDA)," *IEEE Open Journal of Antennas and Propagation*, vol. 2, pp. 1184-1193, 2021.
- [13] E. Yetisir, N. Ghalichechian, and J. L. Volakis, "Ultrawideband Array with 70° scanning using FSS superstrate," *IEEE Transactions on Antennas and Propagation*, vol. 64, no. 10, pp. 4256-4265, 2016.
- [14] J. P. Doane, K. Sertel, J. L. Volakis, and A. Wideband, "A wideband, wide scanning tightly coupled dipole array with integrated balun (TCDA-IB)," *IEEE Transactions on Antennas and Propagation*, vol. 61, no. 9, pp. 4538-4548, 2013.
- [15] J. Shen, C. Zhang, S. Duan, and N. Shao, "Design of a tightly coupled ultra-wideband dual polarization phased array antenna," in *Proceedings of the 2020 International Conference on Microwave and Millimeter Wave Technology (ICMMT)*, pp. 1-3, IEEE, Shanghai, China, September 2020.
- [16] I. Tzanidis, K. Sertel, and J. L. Volakis, "Interwoven Spiral Array (ISPA) With a 10:1 Bandwidth on a Ground Plane," *IEEE Antennas Wirel. Propag. Lett.* vol. 10, pp. 115-118, 2011.
- [17] D. K. Papantonis and J. L. Volakis, "Dual-polarized tightly coupled array with substrate loading," *IEEE Antennas and Wireless Propagation Letters*, vol. 15, pp. 325-328, 2016.
- [18] W. F. Moulder, K. Sertel, and J. L. Volakis, "Superstrate-enhanced Ultrawideband tightly coupled array with resistive FSS," *IEEE Transactions on Antennas and Propagation*, vol. 60, no. 9, pp. 4166-4172, 2012.
- [19] T. R. Vogler, "Analysis of the Radiation Mechanisms in and Design of Tightly-Coupled Antenna Arrays," 2010, <https://vtechworks.lib.vt.edu/handle/10919/29282>.
- [20] Y. Ye, Z. Huang, Y. Jiang et al., "A wideband and wide scanning tightly coupled dipole array with meta-surface wide-angle impedance matching," *Applied Computational Electromagnetics Society*, vol. 36, no. 7, pp. 872-878, 2021.
- [21] Eccofloat, 2021, <http://www.trelleborg.com/en/offshore/products-and-applications/subsea-operations-protected-by-njord-njord-buoyancy/eccofloat>.
- [22] B. Saidaiah, A. Sudhakar, and K. P. Raju, "Modeling and analysis of an efficient bow-tie antenna for UWB applications," in *Proceedings of the 2009 International Conference on Advances in Computing, Control, and Telecommunication Technologies*, pp. 376-379, IEEE, Bangalore, India, December 2009.
- [23] D. A. A. El-Aziz, T. G. Abouelnaga, E. A. Abdallah, M. El-Said, and Y. S. E. Abdo, "Analysis and design of UHF bow-tie RFID tag antenna input impedance," *Open Journal of Antennas and Propagation*, vol. 04, no. 02, pp. 85-107, 2016.
- [24] L. Josefsson and P. Persson, *Conformal Array Antenna Theory and Design*, Wiley-IEEE Press, New Jersey, United States, 2005.
- [25] E. Irci, *Low-Profile Wideband Antennas Based on Tightly Coupled Dipole and Patch Elements* The Ohio State University, Coloumbus, United States, 2011, https://etd.ohiolink.edu/apexprod/rws_olink/r/1501/10?clear=10&p10_accession_num=osu1316456337.
- [26] R. N. Pack, A. S. Brannon, and D. S. Filipovic, "Tightly coupled array of horizontal dipoles over a ground plane," *IEEE Transactions on Antennas and Propagation*, vol. 68, no. 3, pp. 2097-2107, 2020.
- [27] M. Fallah, A. H. Nazeri, M. R. Azadkhan, M. Fallah, A. H. Nazeri, and M. R. Azadkhan, "A novel fractal multiband frequency selective surface," *Journal of Microwaves, Optoelectronics and Electromagnetic Applications*, vol. 18, no. 2, pp. 276-285, 2019.
- [28] O. Luukkonen, C. Simovski, G. Granet et al., "Simple and accurate analytical model of planar grids and high-impedance surfaces comprising metal strips or patches," *IEEE Transactions on Antennas and Propagation*, vol. 56, no. 6, pp. 1624-1632, 2008.
- [29] D. Jackson and N. Alexopoulos, "Gain enhancement methods for printed circuit antennas," *IEEE Transactions on Antennas and Propagation*, vol. 33, no. 9, pp. 976-987, 1985.
- [30] D. R. Jackson and A. A. Oliner, "A leaky-wave analysis of the high-gain printed antenna configuration," *IEEE Transactions on Antennas and Propagation*, vol. 36, no. 7, pp. 905-910, 1988.
- [31] J. Zhong, A. Johnson, E. Alwan, and J. Volakis, "Dual-linear polarized phased array with 9:1 bandwidth and 60° scanning off broadside | IEEE journals & magazine | IEEE xplore," *IEEE*

- Transactions on Antennas and Propagation*, vol. 67, no. 3, 2021, <https://ieeexplore.ieee.org/document/8606988>.
- [32] D. K. Papantoni, E. Yetisir, and J. L. Volakis, "Tightly-coupled array with tunable BW using reconfigurable FFS/superstrate," in *Proceedings of the 2016 USNC-URSI Radio Science Meeting*, pp. 13-14, IEEE, Fajardo, PR, USA, June 2016.
- [33] W. Fuscaldo, P. Burghignoli, P. Baccarelli, and A. Galli, "A reconfigurable substrate-superstrate graphene-based leaky-wave THz antenna," *IEEE Antennas and Wireless Propagation Letters*, vol. 15, pp. 1545-1548, 2016.
- [34] W. Fuscaldo, P. Burghignoli, P. Baccarelli, and A. Galli, "Graphene fabry-perot cavity leaky-wave antennas: plasmonic versus nonplasmonic solutions," *IEEE Transactions on Antennas and Propagation*, vol. 65, no. 4, pp. 1651-1660, 2017.
- [35] 404 - rogers corporation, 2021, <https://www.rogerscorp.com/404>.